Satellite Observations of Precipitating Marine Stratocumulus Show Greater Cloud Fraction for Decoupled Clouds in Comparison to Coupled Clouds

Tom Goren, Daniel Rosenfeld, Odran Sourdeval, Johannes Quaas

AGU100 ADVANCING EARTH AND SPACE SCIENCE

Geophysical Research Letters

RESEARCH LETTER
10.1029/2018GL078122

Key Points:
- A novel satellite-based methodology for retrieving coupling state and thickness of marine warm clouds was developed
- Precipitating decoupled marine stratocumulus have larger cloud fraction compared to similarly precipitating coupled marine stratocumulus
- The coupling state is a potentially important factor in determining the clouds radiative effect

Supporting Information:
- Supporting Information S1

Correspondence to:
T. Goren,
tom.goren@mail.huji.ac.il

Citation:
Goren, T., Rosenfeld, D., Sourdeval, O., & Quaas, J. (2018). Satellite observations of precipitating marine stratocumulus show greater cloud fraction for decoupled clouds in comparison to coupled clouds. *Geophysical Research Letters*, *45*, 5126–5134. https://doi.org/10.1029/2018GL078122

Received 18 FEB 2018
Accepted 23 APR 2018
Accepted article online 8 MAY 2018
Published online 17 MAY 2018

Satellite Observations of Precipitating Marine Stratocumulus Show Greater Cloud Fraction for Decoupled Clouds in Comparison to Coupled Clouds

Tom Goren[1], **Daniel Rosenfeld**[2], **Odran Sourdeval**[1], **and Johannes Quaas**[1]

[1]Institute for Meteorology, Universität Leipzig, Leipzig, Germany, [2]Institute of Earth Sciences, The Hebrew University of Jerusalem, Jerusalem, Israel

Abstract This study examines the relationships between marine stratocumulus clouds (MSC) coupling state with the ocean surface, their precipitation rate and fractional cloud cover (CF). This was possible by developing a novel methodology for satellite retrieval of the clouds coupling state. Decks of overcast MSC were reported in previous studies to break up often as their precipitation rate increases significantly, thus reducing CF and cloud radiative effect substantially. Here we show that decks of precipitating decoupled MSC have larger CF compared to similarly precipitating coupled MSC. The difference in CF between decoupled and coupled clouds was found to increase with precipitation rate, up to nearly doubling the CF of the heaviest precipitating decoupled MSC. This suggests that decoupling is a feature related to higher cloud radiative effect in precipitating MSC.

Plain Language Summary Marine stratocumulus are oceanic clouds that are often observed to exist in two main cloud regimes that differ by their cloud cover. The large cloud cover regime reflects back to space a significant amount of solar energy, in comparison to the low cloud cover regime. Past studies have shown that these cloud cover regimes are related to precipitation rate, so that heavily precipitating clouds often have lower cloud cover than lightly precipitating clouds. In this study we present a novel satellite-based methodology for retrieving the coupling degree (a measure of the interaction between the cloud layer and the ocean's surface) of marine stratocumulus clouds. Such retrievals extend the physical understanding that can be inferred from satellites. We found that heavy precipitation coexists with large cloud cover more often in clouds that are not coupled to the ocean surface. This adds another dimension to the relationship between precipitation rate and cloud cover, and the subsequent effect on the Earth's climate.

1. Introduction

Marine stratocumulus clouds (MSC) cover vast areas of the Earth's ocean surface. Due to their high albedo and large spatial coverage, they affect the radiation balance of the Earth. MSC exhibit different cloud morphologies that can be categorized into (1) homogeneous overcast sheets, (2) closed cells, (3) open cells, and (4) inhomogeneous disorganized cells (Wood & Hartmann, 2006), with the most studied type being open and closed cells (Agee et al., 1973; Atkinson & Zhang, 1996). Closed cells have high cloud fraction (CF) and are driven by radiative cooling from cloud top, which generates a negative buoyancy flux that allows an efficient convective transport of water vapor from the ocean surface into the clouds. Open cells have lower CF and are driven by surface heating and organized by convergence of precipitating-driven downdrafts that spread at the surface (Agee et al., 1973; Atkinson & Zhang, 1996; Berner et al., 2011; Feingold et al., 2010). Precipitation plays a key role in the transition between the two regimes. Under sufficiently low cloud condensation nuclei or high liquid water path (LWP), closed cells start to precipitate (Ackerman et al., 1993; Comstock et al., 2005; Feingold et al., 2010; Goren & Rosenfeld, 2014; Petters et al., 2006; Rosenfeld et al., 2006; Sharon et al., 2006; Stevens et al., 2005; Terai et al., 2014; VanZanten & Stevens, 2005; Wood et al., 2008, 2011). The evaporation of the raindrops below the cloud cools the air and enhances sensible and latent heat fluxes from the ocean surface to the air (Rosenfeld et al., 2006; Stevens et al., 1998; Wang & Feingold, 2009). In addition, precipitation-driven outflows collide and provide additional lifting to the air near the surface (Berner et al., 2011; Feingold et al., 2010; Wang et al., 2010), generating regions of ascent in which precipitating cumulus

form. In accordance, observational and modeling studies have related higher precipitation rate to broken cloud fields, and lower precipitation rate to overcast layers (Kazil et al., 2011; Muhlbauer et al., 2014; Stevens et al., 2005).

A coupled, well-mixed marine boundary layer (MBL), is defined by vertically uniform profile of equivalent potential temperature and total water mixing ratio (Lilly, 1968). When turbulence in the cloud layer is separated from the surface layer, the MBL ceases to be well mixed and becomes decoupled (Nicholls, 1984). Decoupling can be caused by different mechanisms that promote the stratification of the MBL: (1) Solar heating of the cloud layer (Caldwell et al., 2005; Nicholls, 1984; Turton & Nicholls, 2007); (2) precipitation evaporation below cloud base (Caldwell et al., 2005); (3) deepening-warming mechanism: entrainment of dry and warm air from the free troposphere into the MBL that leads to increase in negative subcloud buoyancy fluxes (Bretherton & Wyant, 1997); and (4) advection of clouds over a decreasing sea surface temperature (SST; Stevens et al., 1998).

Here we present a novel method that relies on satellite data for estimating whether cloud updrafts originate at the surface or are detached from it (i.e., coupled or decoupled). The method is used to examine the relationships between the MSC coupling state, precipitation rate, and CF.

2. Data and Methodology

Retrievals from multiple remote sensing instruments on the A-train constellation, complemented with reanalysis data, are used to derive the coupling state of MBL clouds. The A-train is a group of several polar orbiting satellites that follow one another along the same orbital track and provide nearly simultaneous observations of the same location along track. The satellites are crossing the equator at about 1:30 p.m. and 1:30 a.m. local time. Since the method relies on data retrieved from visible sensors, only the noon overpass is used. We used retrievals from the Moderate Resolution Imaging Spectroradiometer (MODIS) satellite for spatial cloud microphysical properties (cloud optical thickness, τ_c; effective radius, r_e; cloud top temperature, T_{cld_top}; and LWP; Cho et al., 2015; Han et al., 1994; Platnick et al., 2003, 2014), while along track retrievals of cloud top height and radar reflectivity were retrieved from the Cloud Aerosol Lidar with Orthogonal Polarization (CALIOP) and CloudSat, respectively (Marchand et al., 2008; Stephens et al., 2002). Spatial meteorological parameters, as well as SST, were provided by the European Center for Medium-Range Weather Forecast (ECMWF) reanalysis (Dee et al., 2011). A detailed description of the data can be found in the supporting information.

The method for retrieving the decoupling degree of boundary layer clouds relies on thermodynamic principles. The main concept is using the retrieved cloud top height and temperature, and the corresponding LWP, to reconstruct the adiabatic thermodynamic profile within and below the cloud, assuming a well-mixed subcloud layer. This provides an adiabatic surface temperature for coupling, T_{adi_sfc}. Assuming that surface sensible heat flux is necessary for coupling the surface and cloud layer, $SST>T_{adi\_sfc}$ indicates mixing and coupling, while $SST<T_{adi\_sfc}$ indicates stability and decoupling. We term $\Delta T_c = T_{adi\_sfc} - SST$ as the decoupling degree, with negative values indicating coupling and positive values indicating decoupling. An evaluation of ΔT_c as a metric for the decoupling degree is presented in section S2, by comparing ΔT_c against the coupling metric used by Comstock et al. (2005), Jones et al. (2011), and Terai and Wood (2013). A correlation of $R^2 = 0.77$ was found between the two metrics for 123 cases that were analyzed, with 80% of the cases being diagnosed with the same coupling state (i.e., coupled or decoupled) by both metrics, suggesting that ΔT_c is a metric that contains similar information compared to the other decoupling metrics.

Figure 1 illustrates the methodology. The initial data are (1) cloud top height ($cloud_{top}$) from CALIOP, (2) satellite-retrieved cloud top temperature (T_{cld_top}), and (3) cloud LWP (LWP_{sat}), both from MODIS, and (4) SST from ECMWF reanalysis. A cloud top pressure of 850 hPa is assumed, given that liquid water mixing ratio lapse rate has low sensitivity to pressure in warm low level clouds (Freud & Rosenfeld, 2012). Using an adiabatic parcel model, the temperature and mixing ratio profiles are calculated from CALIOP-derived cloud top, downwards, in vertical steps of 1 hPa. This provides the vertically integrated liquid water within the cloud, LWP_{adi}, which is used to determine the cloud base height and temperature, where $LWP_{sat} = LWP_{adi}$. Following the initial assumption of a well-mixed subcloud layer, T_{adi_sfc} is calculated assuming a dry adiabatic lapse rate, Γ_d. The decoupling degree is calculated as $\Delta T_c = T_{adi\_sfc} - SST$. The larger the magnitude of ΔT_c, the larger the confidence in whether the clouds are coupled or decoupled, with respect to the negative or positive sign of ΔT_c.

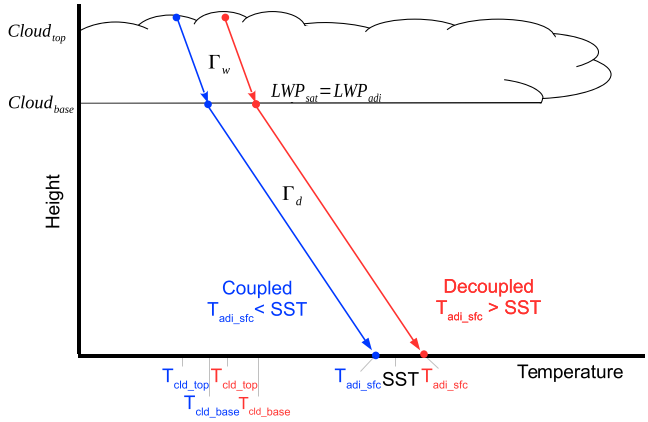

Figure 1. Illustration of the method for satellite retrieval of the decoupling degree of boundary layer clouds over ocean. Cloud top height is retrieved from CALIOP, cloud top temperature and LWP from MODIS, and sea surface temperature (SST) from reanalysis. The temperature and cloud liquid water profiles are calculated from cloud top downwards, assuming adiabaticity and a well-mixed subcloud layer. Cloud base height and temperature are determined to be where the retrieved LWP (LWP_{sat}), is equal to the calculated adiabatic LWP (LWP_{adi}). Clouds are considered to be coupled when $T_{adi\_sfc} < SST$ and decoupled when $T_{adi\_sfc} > SST$. Blue and red arrows illustrate the constructed temperature profiles for coupled and decoupled conditions, respectively. Γ_w and Γ_d are the wet and dry adiabatic temperature lapse rates, respectively. CALIOP = Cloud Aerosol Lidar with Orthogonal Polarization; MODIS = Moderate Resolution Imaging Spectroradiometer.

For the analysis in this study, MODIS swaths were divided into scenes of 100 × 100 km^2, with CALIOP ground track in its center. The decoupling degree was determined for 100 × 100 km^2 scenes using MODIS pixels with τ_c larger than the 95th percentile value in the scene ($\tau_{c,95}$). These pixels are assumed to represent the convective cores, which are the deepest and most active clouds that more closely meet the adiabatic assumption (Goren & Rosenfeld, 2014). Therefore, LWP_{sat} in those pixels can be considered to be more comparable to LWP_{adi}. Assuming that cloud properties change little within an area of 100 × 100 km^2, the mean LWP and T_{cld_top} in the selected $\tau_{c,95}$ pixels were associated to the mean CALIOP cloud top heights, calculated from pixels with tops higher than the 95th percentile value along the 100-km CALIOP ground track in the center of the scene. This was done in order to relate the LWP of the thickest clouds to the clouds with the highest tops. Scenes containing multilayer or ice clouds according to MODIS multi-layer product were excluded. Furthermore, in order to reduce uncertainty in r_e retrievals, pixels with $\tau_c < 5$ were as well excluded (Sourdeval et al., 2015).

Section S2 provides an evaluation of uncertainties associated with LWP, cloud top temperature, pressure, and SST (Donlon et al., 2012; Goren & Rosenfeld, 2014; Sourdeval et al., 2013; Stevens et al., 2007; Zuidema et al., 2009). The propagation of those uncertainties to the ΔT_c standard error ranges from 0.7 to 1 K, with the larger value for thicker clouds. Further discussion can be found in the supporting information.

3. Results

To evaluate the method for retrieving the clouds coupling state we selected a case study from 26 March 2014 under a stationary high pressure system in the south Pacific Ocean. Figure 2 shows the mean sea level pressure, SST and 36-hr back trajectories for several locations around the center of the high pressure. The anticyclonic circulation caused an equatorward and poleward air advection to the east and west of the high pressure, respectively. Accordingly, the eastern section of the high pressure experienced cold advection, while the western section experienced warm advection. Figure 2 also shows MODIS true color image for the same day. The difference in the CF and cloud morphology can be seen between the warm and cold advection regions. While open cells dominate the scene where clouds are advected over warmer SST (i.e., cold advection), overcast is present over the area advected towards colder SST (i.e., warm advection).

3.1. Decoupled Marine Stratocumulus

Figure 3 shows the clouds geometrical, microphysical, and thermodynamical properties as retrieved by the method. The upper panel (Figure 3a) shows the decoupling degree of the clouds, where a positive ΔT_c can be seen. Positive ΔT_c indicates that updrafts at the base of the clouds are decoupled from the ocean surface; hence, the clouds are decoupled. The decoupling degree, as evident by the magnitude of ΔT_c, is stronger

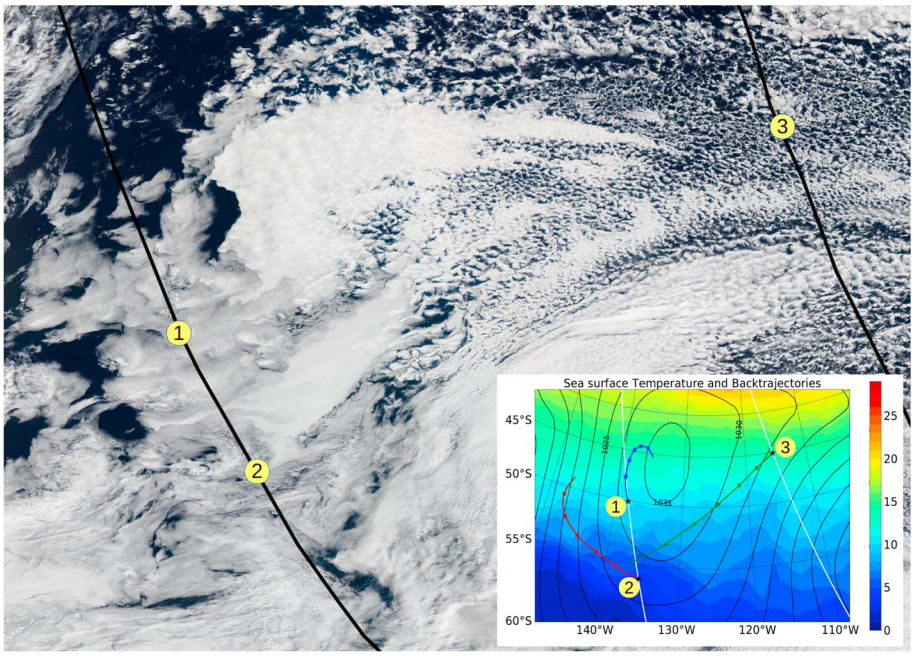

Figure 2. MODIS true color image for 26 March 2014. Overlaid in black lines are CALIOP ground tracks corresponding to approximately 22:00 and 23:35 UTC for the eastern and western tracks, respectively. The numbers represent the ending point of back trajectories. The image scales to $\pm$3,500 $\times$ 3,500 km^2. Bottom right: sea surface temperature and sea level pressure for the same day. The colored lines represent 36-hr back trajectories with ticks every 6 hr. The stars represent the ending point of the back trajectories along the CALIOP ground track (white lines). CALIOP = Cloud Aerosol Lidar with Orthogonal Polarization; MODIS = Moderate Resolution Imaging Spectroradiometer.

in the south and weaker in the north of the scene. Examining the Lagrangian back trajectories of the clouds during the previous 36 hr provides the reason. It can be seen in Figure 2 that trajectory 2, which represents the clouds with the stronger decoupling, was advected over a decreasing SST for a longer time and over a stronger temperature gradient than trajectory 1. As a result, the boundary layer air traveling along trajectory 2 became more stable and therefore more strongly decoupled.

Observational and modeling studies found a threshold r_e for significant drizzle of 14–16 μm (Freud & Rosenfeld, 2012; Gerber, 1996; Han et al., 1995; Rosenfeld et al., 2012; VanZanten & Stevens, 2005). Figures 3b and 3c show CloudSat reflectivity factor and MODIS r_e, where it can be seen that stronger reflectivity is present where $r_e > 15$ μm. Such MSC are expected to exist in the form of open cells (Ackerman et al., 1993; Comstock et al., 2005; Feingold et al., 2010; Rosenfeld et al., 2006; Sharon et al., 2006; Stevens et al., 2005; VanZanten & Stevens, 2005; Wood et al., 2011). In this case, however, apart from limited clearing around point 2 in Figure 3e, the clouds remained overcast.

The radar reflectivity of the clouds is rather low (Figure 3b), presumably because the clouds lose cloud water to rain without replenishment of moisture from the ocean surface. This can explain the low LWP on the order of ~50 g/m^2 (Figure 3d), in accordance with previous observations of LWP in decoupled MSC (Han et al., 2002). Lower LWP acts to weaken turbulent kinetic energy production in the cloud layer and thus to reduce mixing and entrainment of dry air from the free troposphere (Stevens et al., 1998; Wood, 2007). Weaker turbulence may explain the smooth texture of the decoupled layer and the absence of closed-cell structure (Figure 2). Weaker entrainment possibly slows the evaporation of the cloud, which may result in a longer cloud lifetime. In accordance, a trajectory analysis of the air mass in which the decoupled clouds were observed shows that after approximately 24 hr the clouds remained overcast (section S3).

3.2. Coupled Marine Stratocumulus

On the eastern side of the high pressure system clouds were advected equatorward over increasing SST (trajectory 3 in Figure 2). Figure 4 shows the cloud geometrical, microphysical, and thermodynamical properties of the coupled clouds in that region. It can be seen that open cells dominate most of the region, and, as expected, the r_e is larger than 15 μm (Figure 4c). Strong radar reflectivity (up to 5 dBZ) is detected by CloudSat

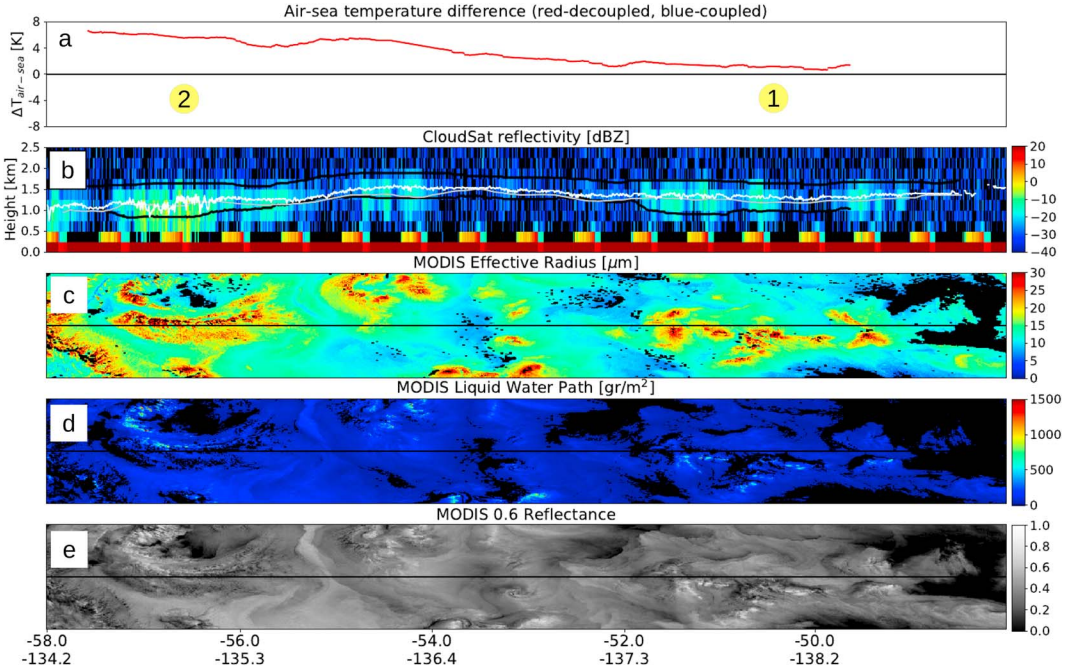

Figure 3. Satellite retrieval of the cloud geometrical, microphysical, and thermodynamical properties. (a) ΔT_c as an indication for the decoupling degree of the clouds. Positive ΔT_c (red line) indicates that the clouds are decoupled from the surface. Negative ΔT_c (blue line, not observed in this case) indicates that the clouds are coupled to the surface. Numbers represent the location of the ending point of the back trajectories (see Figure 2); (b) CloudSat reflectivity profile and cloud top and base heights. Upper and lower black lines represent CALIOP cloud top and calculated cloud base, respectively, over a running window of 100×100 km^2. Gray line is cloud base that is calculated only for MODIS pixels that collocate directly with CALIOP cloud top height, averaged over a running window of 20 km. White line is CALIOP deepest penetration depth before a complete extinction of the laser beam, which constrains the highest possible cloud base height; (c) MODIS r_e; (d) MODIS LWP; and (e) Reflectivity at 0.65 μm. Horizontal lines in (c)–(e) represent the location of CALIOP ground track. The width of panels (c)–(e) is 300 km. CALIOP = Cloud Aerosol Lidar with Orthogonal Polarization; LWP = liquid water path; MODIS = Moderate Resolution Imaging Spectroradiometer.

(Figure 4b), indicating heavy drizzle. The clouds are not broken only in a small area near 44°S, where r_e is very close to 15 μm and precipitate only lightly. This is consistent with the notion that clouds break up in response to precipitation when r_e exceeds 15 μm. The coupling of the clouds (Figure 4a) possibly allows aerosols from the ocean surface to reach the cloud layer and to maintain the modest cloud condensation nuclei concentration that is important for preventing the heavily precipitating cumulus field from collapsing (Ackerman et al., 1993; Wang et al., 2010; Wood et al., 2015).

4. Statistical Analysis

In order to provide a statistical corroboration of the relationships between coupling state, precipitation rate and CF, 162 MODIS swaths with no preferable season were analyzed. Each MODIS swath was divided into scenes of 100×100 km^2, with the CALIOP ground track at the center of the scenes. Scenes were required to satisfy the following conditions: (1) between latitude 60°S and 60°N, (2) have a scene mean top height <3 km, and (3) containing a homogeneous cloud regime; this was done by dividing the surrounding 300×300 km^2 region into smaller 3×3 regions of 100×100 km^2, and calculating their CF; a standard deviation < 0.15 among the nine smaller regions was considered homogeneous. A total of 563 coupled and 130 decoupled scenes of 100×100 km^2 were found. Among those 216 and 54 coupled and decoupled scenes, respectively, were found to have a scene mean dBZ > 0. Following Muhlbauer et al. (2014), dBZ > 0 indicates on heavy precipitation and marks the difference in rain intensities between overcast closed cells and broken open cells.

Figures 5a and 5b show box-plot diagrams of CF and CloudSat reflectivity for precipitating (dBZ > 0) coupled and decoupled clouds. A significant difference in CF can be seen between the two groups, with 55% and 80% mean CF for the coupled and decoupled clouds, respectively (Figure 5a). This indicates that precipitating decoupled clouds are less frequently found to have low CF. CloudSat reflectivities in decoupled and

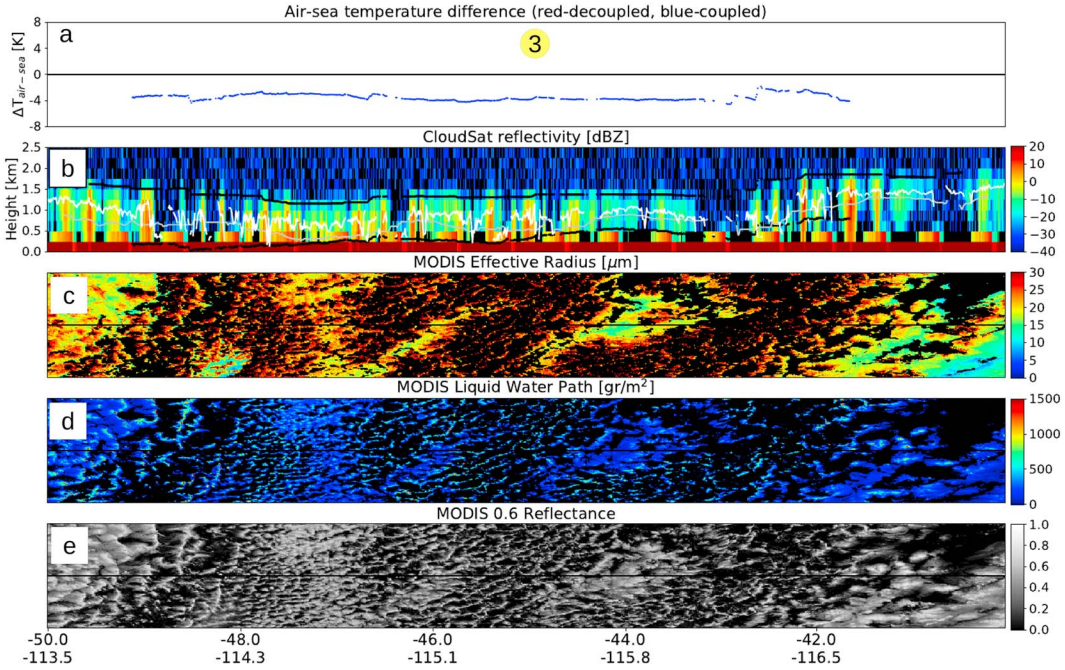

Figure 4. Same as Figure 3 but for coupled clouds.

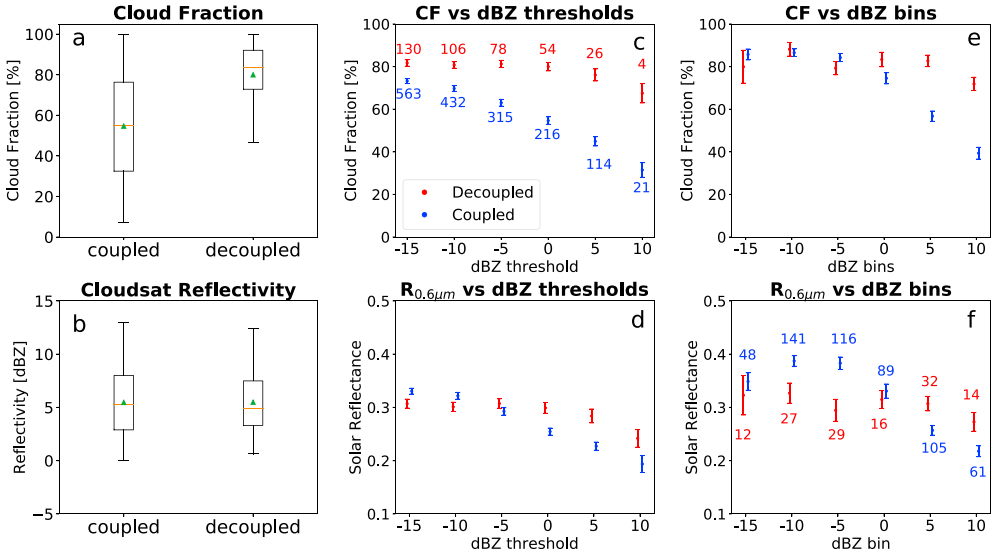

Figure 5. (a and b) Box plots of cloud fraction (CF) and cloudSat radar reflectivity of precipitating (dBZ > 0) coupled and decoupled MSC cloud scenes of 100 × 100 km^2. The boxes extend vertically from the 25th to the 75th percentile of the data, with the median shown by the horizontal orange line in the box interior, and the whiskers extend out to the most extreme values. Triangles represent the mean. CF in each 100 × 100 km^2 region was determined by the fraction of pixels with a successfully retrieved τ_c. dBZ reflectivities represent along track data, at the center of the scene, averaged from the maximum dBZ within each column that is larger than the 95th percentile value of the columns maximum dBZ within the scene, in consistency with the other cloud properties (see section 2). (c–f) Average CF (c and e) and 0.6 μm solar reflectance (d and f) for varying minimum CloudSat reflectivity thresholds and bins. Overlaid numbers represent the number of scenes for each dBZ threshold or bin, for coupled and decoupled cases. Bars represent the standard error. Figure S4 provides a box-plot representation of (c) and (d). Table S6 provides additional statistical characteristics of coupled and decoupled clouds, including meteorological parameters (Klein & Hartmann, 1993; Lawrence, 2005; Sandu et al., 2010).

coupled clouds share a similar distribution (Figure 5b), suggesting that relatively high rain rates can occur also in decoupled clouds, only that the cloud roots are not coupled to the surface. In such cases advection of warm humid air possibly provides the moisture needed for the precipitation.

Figures 5c–5f show the average CF and 0.6 μm solar reflectance ($R_{0.6}$) for varying CloudSat radar reflectivity thresholds and interval bins. The dBZ thresholds provide an overall bulk assessment of the differences between coupled and decoupled clouds, while the interval bins provide a more detailed understanding regarding the role of precipitation intensity. Figure 5c shows that the CF of decoupled clouds decreases only slightly with increasing dBZ from −15 to +5 dBZ, while the CF of coupled clouds decreases more rapidly. The difference in CF is largest when the heaviest rainfall occurs, as indicated by the higher reflectivities. This means that stronger precipitation rate is less associated with lower CF when clouds are decoupled. Figure 5e shows that the difference in CF becomes significant only when dBZ ≥ 0, suggesting that transitions from closed to open cells in coupled clouds, that occur when precipitation rate crosses the dBZ = 0 threshold (Muhlbauer et al., 2014) possibly explain the observed CF difference.

The scene mean $R_{0.6}$ presents a more complex behavior (Figures 5d and 5f). The difference in $R_{0.6}$ between decoupled and coupled clouds changes its sign from negative to positive as dBZ increases. At low dBZ coupled and decoupled clouds have similar CF (Figures 5c and 5e), and the lower $R_{0.6}$ in decoupled clouds can be attributed to their lower LWP (Figure S5). The lower LWP in decoupled clouds is likely a result of limited moisture supply from the ocean surface due to the decoupling. It is also possible that the decoupling prevents aerosols from the surface reaching the clouds, which therefore have less, but larger cloud droplets, and subsequently lower $R_{0.6}$ (Twomey, 1977). As precipitation rate increases, the larger $R_{0.6}$ of coupled clouds is being eroded due to the decrease in CF, so that $R_{0.6}$ of decoupled clouds becomes comparably larger. For a dBZ threshold larger than 0, $R_{0.6}$ in decoupled clouds was found to be higher by nearly 20% in comparison to similarly precipitating coupled clouds (Figure 5d and Table S6). This suggests that decoupling is a property associated with larger cloud radiative effect in precipitating MSC.

5. Summary

The observations presented here show that precipitating decoupled MSC have larger CF compared to similarly precipitating coupled MSC. Heavily precipitating (dBZ > 0) decoupled MSC were found to be associated with higher shortwave reflectance, suggesting that the coupling state is a potentially important feature characterizing cloud radiative effect in precipitating MSC. The results are based on a novel satellite-based methodology for retrieving the coupling state and thickness of marine boundary layer clouds. The causality between coupling state, precipitation rate, and CF could not be fully addressed in this study. Nevertheless, the observed difference in CF between coupled and decoupled clouds, which was found to be the largest when the heaviest rainfall occurs (Figures 5c and 5e), supports the case study presented in section 3 and suggests that decoupling may prevent precipitation-related breakup. Following this, we hypothesize a mechanism, in which under strongly decoupled conditions, the dynamical forcing from precipitation-driven downdrafts that spread at the surface into colliding gust fronts (Feingold et al., 2010; Wang et al., 2010) is not sufficient to recouple the MBL and to create cumulus convection that breaks up the stratocumulus deck. Alternatively, the downdrafts do not descend all the way to the surface due to the stability there, thus not forming gust fronts. As a result, the cloud breakup may be prevented. The hypothesis can be tested by targeting the critical questions in future field campaigns and large eddy simulations.

Acknowledgments
T. G. received funding from the European Union Horizon 2020 research and innovation programme under the Marie Sklodowska-Curie grant agreement 703880. J. Q. acknowledges funding by the European Research Council, starting grant 306284 "QUAERERE." We thank Edward Gryspeerdt and Johannes Mülmenstädt for helpful conversations and support. Satellite and reanalysis data that were used in this study are available to download per request by the following online ordering data systems: MODIS and CALIOP (http://reverb.echo.nasa.gov/); CloudSat (http://www.cloudsat.cira.colostate.edu/); ECMWF (http://www.ecmwf.int/); and MODIS true-color images (https://worldview.earthdata.nasa.gov/). HYSPLIT back trajectories can be computed online (http://ready.arl.noaa.gov). A detailed description of the data that were used in the study can be found in the supporting information.

References

Ackerman, A. S., Toon, O. B., & Hobbs, P. V. (1993). Dissipation of marine stratiform clouds and collapse of the marine boundary layer due to the depletion of cloud condensation nuclei by clouds. *Science*, *262*(5131), 226–229. https://doi.org/10.1126/science.262.5131.226

Agee, E. M., Chen, T. S., & Dowell, K. E. (1973). A review of mesoscale cellular convection. *Bulletin of the American Meteorological Society*, *54*(10), 1004–1012. https://doi.org/10.1175/1520-0477(1973)054<1004:AROMCC>2.0.CO;2

Atkinson, B. W., & Zhang, J. (1996). Mesoscale shallow convection in the atmosphere. *Reviews of Geophysics*, *34*(4), 403–431. https://doi.org/10.1029/96RG02623

Berner, A. H., Bretherton, C. S., & Wood, R. (2011). Large-eddy simulation of mesoscale dynamics and entrainment around a pocket of open cells observed in VOCALS-REx RF06. *Atmospheric Chemistry and Physics*, *11*(20), 10,525–10,540. https://doi.org/10.5194/acp-11-10525-2011

Bretherton, C. S, & Wyant, M. C. (1997). Moisture transport, lower-tropospheric stability, and decoupling of cloud-topped boundary layers. *Journal of the Atmospheric Sciences*, *54*(1), 148–167. https://doi.org/10.1175/1520-0469(1997)054<0148:MTLTSA>2.0.CO;2

Caldwell, P., Bretherton, C. S., & Wood, R. (2005). Mixed-layer budget analysis of the diurnal cycle of entrainment in Southeast Pacific stratocumulus. *Journal of the Atmospheric Sciences*, *62*(10), 3775–3791. https://doi.org/10.1175/JAS3561.1

Cho, H.-M., Zhang, Z., Meyer, K., Lebsock, M., Platnick, S., Ackerman, A. S., et al. (2015). Frequency and causes of failed MODIS cloud property retrievals for liquid phase clouds over global oceans. *Journal of Geophysical Research: Atmospheres*, *120*, 4132–4154. https://doi.org/10.1002/2015JD023161

Comstock, K. K., Bretherton, C. S., & Yuter, S. E. (2005). Mesoscale variability and drizzle in Southeast Pacific stratocumulus. *Journal of the Atmospheric Sciences*, *62*(10), 3792–3807. https://doi.org/10.1175/JAS3567.1

Dee, D. P., Uppala, S. M., Simmons, A. J., Berrisford, P., Poli, P., Kobayashi, S., et al. (2011). Others The ERA-Interim reanalysis: Configuration and performance of the data assimilation system. *Quarterly Journal of the Royal Meteorological Society*, *137*(656), 553–597.

Donlon, C. J., Martin, M., Stark, J., Roberts-Jones, J., Fiedler, E., & Wimmer, W. (2012). The operational sea surface temperature and sea ice analysis (OSTIA) system. *Remote Sensing of Environment*, *116*, 140–158. https://doi.org/10.1016/j.rse.2010.10.017

Feingold, G., Koren, I., Wang, H., Xue, H., & Brewer, W. A. (2010). Precipitation-generated oscillations in open cellular cloud fields. *Nature*, *466*(7308), 849–852. https://doi.org/10.1038/nature09314

Freud, E., & Rosenfeld, D. (2012). Linear relation between convective cloud drop number concentration and depth for rain initiation. *Journal of Geophysical Research*, *117*, D02207. https://doi.org/10.1029/2011JD016457

Gerber, H. (1996). Microphysics of marine stratocumulus clouds with two drizzle modes. *Journal of Atmospheric Sciences*, *53*(12), 1649–1662. https://doi.org/10.1175/1520-0469(1996)053<1649:MOMSCW>2.0.CO;2

Goren, T., & Rosenfeld, D. (2014). Decomposing aerosol cloud radiative effects into cloud cover, liquid water path and Twomey components in marine stratocumulus. *Atmospheric Research*, *138*, 378–393. https://doi.org/10.1016/j.atmosres. 2013.12.008

Han, Q., Rossow, W. B., & Lacis, A. A. (1994). Near-global survey of effective droplet radii in liquid water clouds using ISCCP data. *Journal of Climate*, *7*(4), 465–497.

Han, Q., Rossow, W. B., Zeng, J., & Welch, R. (2002). Three different behaviors of liquid water path of water clouds in aerosol cloud interactions. *Journal of the Atmospheric Sciences*, *59*(3), 726–735. https://doi.org/10.1175/1520-0469(2002)059<0726:TDBOLW>2.0.CO;2

Han, Q., Welch, R., Chou, J., Rossow, W., & White, A. (1995). Validation of satellite retrievals of cloud microphysics and liquid water path using observations from FIRE. *Journal of the Atmospheric Sciences*, *52*(23), 4183–4195. https://doi.org/10.1175/1520-0469(1995)052<4183:VOSROC>2.0.CO;2

Jones, C. R., Bretherton, C. S., & Leon, D. (2011). Coupled vs. decoupled boundary layers in VOCALS-REx. *Atmospheric Chemistry and Physics*, *11*(14), 7143–7153. https://doi.org/10.5194/acp-11-7143-2011

Kazil, J., Wang, H., Feingold, G., Clarke, a. D., Snider, J. R., & Bandy, a. R. (2011). Modeling chemical and aerosol processes in the transition from closed to open cells during VOCALS-REx. *Atmospheric Chemistry and Physics*, *11*(15), 7491–7514. https://doi.org/10.5194/acp-11-7491-2011

Klein, S. A., & Hartmann, D. L. (1993). The seasonal cycle of low stratiform clouds. *Journal of Climate*, *6*(8), 1587–1606.

Lawrence, M. G. (2005). The relationship between relative humidity and the dewpoint temperature in moist air: A simple conversion and applications. *Bulletin of the American Meteorological Society*, *86*(2), 225–233. https://doi.org/10. 1175/BAMS-86-2-225

Lilly, D. K. (1968). Models of cloud-topped mixed layers under a strong inversion. *Quarterly Journal of the Royal Meteorological Society*, *94*(401), 292–309. https://doi.org/10.1002/qj.49709440106

Marchand, R., Mace, G. G., Ackerman, T., & Stephens, G. (2008). Hydrometeor detection using Cloudsat: An earth-orbiting 94-GHz cloud radar. *Journal of Atmospheric and Oceanic Technology*, *25*(4), 519–533. https://doi.org/10.1175/2007JTECHA1006.1

Muhlbauer, A., McCoy, I. L., & Wood, R. (2014). Climatology of stratocumulus cloud morphologies: Microphysical properties and radiative effects. *Atmospheric Chemistry and Physics*, *14*, 6695–6716. https://doi.org/10. 5194/acp-14-6695-2014

Nicholls, S. (1984). The dynamics of stratocumulus: Aircraft observations and comparisons with a mixed layer model. *Quarterly Journal of the Royal Meteorological Society*, *110*(466), 783–820. https://doi.org/10.1002/qj.49711046603

Petters, M. D., Snider, J. R., Stevens, B., Vali, G., Faloona, I., & Russell, L. M. (2006). Accumulation mode aerosol, pockets of open cells, and particle nucleation in the remote subtropical Pacific marine boundary layer. *Journal of Geophysical Research*, *111*, D02206. https://doi.org/10.1029/2004JD005694

Platnick, S., King, M., Ackerman, S., Menzel, W., Baum, B., Riedi, J., & Frey, R. (2003). The MODIS cloud products: Algorithms and examples from terra. *IEEE Transactions on Geoscience and Remote Sensing*, *41*(2), 459–473. https://doi.org/10.1109/TGRS.2002.808301

Platnick, S., King, M. D., Meyer, K. G., Wind, G., Amarasinghe, N., Marchant, B., et al. (2014). Others MODIS cloud optical properties: User guide for the Collection 6 Level-2 MOD06/MYD06 product and associated Level-3 Datasets. Version 0.9, 17.

Rosenfeld, D., Kaufman, Y. J., & Koren, I. (2006). Switching cloud cover and dynamical regimes from open to closed Benard cells in response to the suppression of precipitation by aerosols. *Atmospheric Chemistry and Physics*, *6*(9), 2503–2511. https://doi.org/10.5194/acp-6-2503-2006

Rosenfeld, D., Wang, H., & Rasch, P. J. (2012). The roles of cloud drop effective radius and LWP in determining rain properties in marine stratocumulus. *Geophysical Research Letters*, *39*, L13801. https://doi.org/10.1029/2012GL052028

Sandu, I., Stevens, B., Pincus, R., & Angeles, L. (2010). On the transitions in marine boundary layer cloudiness. *Atmospheric Chemistry and Physics*, *10*, 2377–2391. https://doi.org/10.5194/acp-10-2377-2010

Sharon, T. M., Albrecht, B. A., Jonsson, H. H., Minnis, P., Khaiyer, M. M., van Reken, T. M., et al. (2006). Aerosol and cloud microphysical characteristics of rifts and gradients in maritime stratocumulus clouds. *Journal of the Atmospheric Sciences*, *63*(3), 983–997. https://doi.org/10.1175/JAS3667.1

Sourdeval, O., Labonnote, L. C., Baran, A. J., & Brogniez, G. (2015). A methodology for simultaneous retrieval of ice and liquid water cloud properties. Part I: Information content and case study. *Quarterly Journal of the Royal Meteorological Society*, *141*(688), 870–882. https://doi.org/10.1002/qj.2405

Sourdeval, O., Labonnote, L. C., Brogniez, G., Jourdan, O., Pelon, J., & Garnier, A. (2013). A variational approach for retrieving ice cloud properties from infrared measurements: Application in the context of two IIR validation campaigns. *Atmospheric Chemistry and Physics*, *13*(16), 8229–8244.

Stephens, G. L., Vane, D. G., Boain, R. J., Mace, G. G., Sassen, K., Wang, Z., et al. (2002). Others The CloudSat mission and the A-Train: A new dimension of space-based observations of clouds and precipitation. *Bulletin of the American Meteorological Society*, *83*(12), 1771–1790.

Stevens, B., Beljaars, A., Bordoni, S., Holloway, C., Köhler, M., Krueger, S., et al. (2007). On the structure of the lower troposphere in the summertime stratocumulus regime of the Northeast Pacific. *Monthly Weather Review*, *135*(3), 985–1005. https://doi.org/10.1175/MWR3427.1

Stevens, B, Cotton, W. R., & Feingold, G. (1998). Large-Eddy simulations of strongly precipitating, shallow, stratocumulus-topped boundary layers. *Journal of the Atmospheric*, *55*, 3616–3638. https://doi.org/10.1175/1520-0469(1998)055<3616:LESOSP>2.0.CO;2

Stevens, B., Vali, G., Comstock, K., Wood, R., Van Zanten, M. C., Austin, P. H., et al. (2005). Pockets of open cells and drizzle in marine stratocumulus. *Bulletin of the American Meteorological Society*, *86*(1), 51–57. https://doi.org/10.1175/BAMS-86-1-51

Terai, C. R., Bretherton, C. S., Wood, R., & Painter, G. (2014). Aircraft observations of aerosol, cloud, precipitation, and boundary layer properties in pockets of open cells over the southeast Pacific. *Atmospheric Chemistry and Physics*, *14*(15), 8071–8088. https://doi.org/10.5194/acp-14-8071-2014

Terai, C. R., & Wood, R. (2013). Aircraft observations of cold pools under marine stratocumulus. *Atmospheric Chemistry and Physics*, *13*(19), 9899–9914.

Turton, J. D., & Nicholls, S. (2007). A study of the diurnal variation of stratocumulus using a multiple mixed layer model. *Quarterly Journal of the Royal Meteorological Society*, *113*(477), 969–1009. https://doi.org/10.1002/qj.49711347712

Twomey, S. (1977). The influence of pollution on the shortwave albedo of clouds. *Journal of the Atmospheric Sciences*, *34*(7), 1149–1152.

VanZanten, M. C., & Stevens, B. (2005). Observations of the structure of heavily precipitating marine stratocumulus. *Journal of the Atmospheric Sciences*, *62*(12), 4327–4342. https://doi.org/10.1175/JAS3611.1

Wang, H., & Feingold, G. (2009). Modeling mesoscale cellular structures and drizzle in marine stratocumulus. Part I: Impact of drizzle on the formation and evolution of open cells. *Journal of the Atmospheric Sciences*, *66*(11), 3237–3256. https://doi.org/10.1175/2009JAS3022.1

Wang, H., Feingold, G., Wood, R., & Kazil, J. (2010). Modelling microphysical and meteorological controls on precipitation and cloud cellular structures in Southeast Pacific stratocumulus. *Atmospheric Chemistry and Physics*, *10*(13), 6347–6362. https://doi.org/10.5194/acp-10-6347-2010

Wood, R. (2007). Cancellation of aerosol indirect effects in marine stratocumulus through cloud thinning. *Journal of the Atmospheric Sciences*, *64*(7), 2657–2669. https://doi.org/10.1175/JAS3942.1

Wood, R., Bretherton, C. S., Leon, D., Clarke, a. D., Zuidema, P., Allen, G., & Coe, H. (2011). An aircraft case study of the spatial transition from closed to open mesoscale cellular convection over the Southeast Pacific. *Atmospheric Chemistry and Physics*, *11*(5), 2341–2370. https://doi.org/10.5194/acp-11-2341-2011

Wood, R., Comstock, K. K., Bretherton, C. S., Cornish, C., Tomlinson, J., Collins, D. R., & Fairall, C. (2008). Open cellular structure in marine stratocumulus sheets. *Journal of Geophysical Research*, *113*, D12207. https://doi.org/10.1029/2007JD009371

Wood, R., & Hartmann, D. L. (2006). Spatial variability of liquid water path in marine low cloud: The importance of mesoscale cellular convection. *Journal of Climate*, *19*(9), 1748–1764.

Wood, R., Wyant, M., Bretherton, C. S., Rèmillard, J., Kollias, P., Fletcher, J., et al. (2015). Clouds, aerosols, and precipitation in the marine boundary layer: An arm mobile facility deployment. *Bulletin of the American Meteorological Society*, *96*(3), 419–439. https://doi.org/10.1175/BAMS-D-13-00180.1

Zuidema, P., Painemal, D., de Szoeke, S., & Fairall, C. (2009). Stratocumulus cloud-top height estimates and their climatic implications. *Journal of Climate*, *22*(17), 4652–4666. https://doi.org/10.1175/2009JCLI2708.1